Charge and matter radial distributions of heavy-light mesons calculated on a lattice

A. M. Green,* J. Koponen,† and P. Pennanen‡

Department of Physical Sciences and Helsinki Institute of Physics, P. O. Box 64, FIN-00014 University of Helsinki, Finland

C. Michael§

Department of Mathematical Sciences, University of Liverpool, L69 3BX, United Kingdom

(UKQCD Collaboration)

For a heavy-light meson with a static heavy quark, we can explore the light quark distribution. The charge and matter radial distributions of these heavy-light mesons are measured on a $16^3 \times 24$ lattice at $\beta = 5.7$ and a hopping parameter corresponding to a light quark mass about that of the strange quark. Both distributions can be well fitted up to 4 lattice spacings ($r \approx 0.7$ fm) with the exponential form $w_i^2(r)$, where $w_i(r) = A \exp(-r/r_i)$. For the charge (c) and matter (m) distributions $r_c \approx 0.32(2)$ fm and $r_m \approx 0.24(2)$ fm. We also discuss the normalization of the total charge and matter integrated over all space, finding 1.30(5) and 0.4(1), respectively.

I. INTRODUCTION

Lattice QCD has had considerable success in the understanding of the energies of few-quark systems. However, the spatial distributions of the quarks in these systems have received much less attention. The reasons for this are twofold. First, unlike energies, these distributions are not directly observable, but arise only in integrated forms such as sum rules, form factors, transition rates etc. Secondly, as will be seen later, their measurement on a lattice is more difficult and less accurate than that of the corresponding energies. In spite of this, it is of interest to extract lattice estimates of various spatial distributions and this is the aim of the present study.

There have been earlier lattice measurements of radial distributions. However, they differ from the present work in several ways. For example, in Ref. [1] the authors are interested in the coupling between B mesons and the π, which involves a pseudovector coupling of the π to a single quark. In contrast, here it is the charge and matter distributions that are studied and these involve vector and scalar couplings. Scalar coupling to single quarks was also studied in Refs. [2,3]. However, there only the scalar sum rule was evaluated, since that was primary a study of the dependence of the meson mass on the quark masses.

A knowledge of spatial distributions can be utilized in a variety of ways. For example, the charge distribution of the light quark ($\bar{q}$) in a heavy-light meson ($Q\bar{q}$) can be used to check possible potential models, where the distributions are calculated from wave functions generated by some differential equation containing an interquark potential V. In such models [4] there are several uncertainties—the form of V, the

form of the differential equation, how to include relativistic effects—some of which are tuned to ensure that the model reproduces the correct ($Q\bar{q}$) energies. The latter can be in several partial waves $S_{1/2}, P_{1/2}, P_{3/2}$, etc., and can be either the observed energies of, for example, the B meson or the results of a lattice calculation. However, if spatial distributions are also known *a priori* from, say, a lattice calculation, then the uncertainties in such potential models will be reduced. Another way that the ($Q\bar{q}$) charge distribution could be of use is in the understanding of multiquark systems. In few-nucleon systems (e.g. ^{3}He, ^{4}He) it is found that the nucleon-nucleon correlations are, at short distances, very similar to that in the *two*-nucleon system—with differences arising at large distances due to the different binding energies [5]. This important observation can then be exploited in models of multinucleon systems, by assuming that the internucleon correlations are dominated by their two-nucleon counterparts. In the corresponding multiquark case it would be of interest if a similar simplification were to arise. Therefore, as a first step in that direction, a knowledge of the two-quark radial correlation in the basic ($Q\bar{q}$) case is needed—to be compared later with those in, say, the (Q^2q) or ($Q^2\bar{q}^2$) system. This probing of the ($Q\bar{q}$) or ($Q^2\bar{q}^2$) structure could be carried to a more fundamental level by measuring the form of the underlying color fields that lead to the interquark potential V and the radial correlations. Such an extension would be analogous to the study of these fields in the ($Q\bar{Q}$) and ($Q^2\bar{Q}^2$) systems—see Refs. [6].

It should be added that the heavy-light system ($Q\bar{q}$) is the quark model equivalent to the hydrogen atom (Pe^-). Therefore, from a general point of view, it is of interest in any discussions comparing the properties of two-body systems constructed from two particles one of which is very much heavier than the other. Also, the interactions in the two cases have common features—the Coulomb potential $\propto e^2/r$ of the hydrogen atom versus the one-gluon exchange $\propto \alpha/r$ in the heavy-light meson.

*Email address: anthony.green@helsinki.fi
†Email address: jmkopone@rock.helsinki.fi
‡Email address: petrus@hip.fi
§Email address: cmi@liv.ac.uk

In Sec. II the maximal variance reduction method, crucial for extracting reliable results, is briefly discussed. In Sec. III the formalism is introduced for evaluating the two- and three-point correlation functions $C(2)$ and $C(3)$. In Sec. IV variational methods for analyzing the lattice data are explained. In Sec. V the results are given and in Sec. VI some conclusions are made.

II. MAXIMUM VARIANCE REDUCTION METHOD

It has been demonstrated that light-quark propagators can be constructed in an efficient way using the so-called maximum variance reduction (MVR) method. Since this has been explained in detail elsewhere, for example in Ref. [7], the emphasis here will be mainly on the differences that arise when estimating on a lattice the correlation functions $C(2), C(3)$ needed for measuring spatial charge and matter densities. In the MVR method the inverse of a positive definite matrix A is expressed in the form of a Monte Carlo integration

$$A_{ji}^{-1} = \frac{1}{Z} \int D\phi \, \phi_i^* \phi_j \exp\left(-\frac{1}{2} \phi^* A \phi \right), \tag{1}$$

where the scalar fields ϕ are pseudofermions located on lattice sites i, j. For a given gauge configuration on this lattice, N independent samples of the ϕ fields can be constructed by Monte Carlo techniques, resulting in a stochastic estimate of A_{ji}^{-1} as an average of these N samples i.e. $A_{ji}^{-1} = \langle \phi_i^* \phi_j \rangle$. The N samples of the ϕ fields can be calculated separately and stored for use in any problem involving light quarks with the same gauge configurations.

In QCD the matrix of interest is the Wilson-Dirac matrix $Q = 1 - \kappa M$, which is not positive definite for those values of the hopping parameter κ that are of interest. Therefore, we must deal with $A = Q^\dagger Q$, which is positive definite. Since M contains only nearest neighbor interactions, A—with at most next-to-nearest neighbor interactions—is still sufficiently local for effective updating schemes to be implemented. In this case the light-quark propagator from site i to site j is expressed as

$$G_q = G_{ji} = Q_{ji}^{-1} = \langle (Q_{ik}\phi_k)^* \phi_j \rangle = \langle \psi_i^* \phi_j \rangle. \tag{2}$$

This is the key element in the following formalism. The Wilson-Dirac matrix also leads to an alternative form for the above light-quark propagator from site i to near site j:

$$G_q' = G_{ji}' = \gamma_5 \langle (Q_{jk}\phi_k)\phi_i^* \rangle \gamma_5 = \gamma_5 \langle \psi_j \phi_i^* \rangle \gamma_5. \tag{3}$$

Later, it will be essential to use at some lattice sites operators that are *purely local*. This then restricts us to using at such sites only the ϕ fields that are located on single lattice sites. In contrast the ψ_i fields—defined as $Q_{ik}\phi_k$—are not purely local, since they contain ϕ fields on next-to-nearest neighbor sites.

In the above, the term "maximal variance reduction" comes from the technique applied to reduce the statistical noise in Eq. (2). The lattice is divided into two boxes (0 $< t < T/2$ and $T/2 < t < T$) whose boundary is kept fixed.

Variance of the pseudofermionic fields is then reduced by numerically solving the equation of motion inside each box. This allows the variance of propagators from one box to the other to be greatly reduced. However, in the case of a three-point correlation two propagators are needed and this is best treated by choosing one of the points to be on the boundary of the boxes while the other two are inside their own boxes. Furthermore, the field at the boundary must be local to avoid the two propagators interfering with each other. This means that only the ϕ fields can be used on the boundary and there they couple to the charge or matter operator. For the points in the boxes, the temporal distance from the boundary should be approximately equal to give the propagators a similar degree of statistical variance.

III. THE CORRELATION FUNCTIONS $C(2)$ AND $C(3)$

In this section an expression is given for evaluating the two-point correlation $C(2)$—needed for extracting the basic $Q\bar{q}$ energies (m_α) and eigenfunctions (v_i^α). As will be discussed in more detail in Sec. IV B, $C(2)$ is expressed in the form of a matrix $C_{ij}(2)$—with rank 3 found to be sufficient. The m_α and v_i^α are then extracted from fitting the $C_{ij}(2,T)$ by the form

$$\sum_{\alpha=1}^{M} v_i^\alpha \exp(-m_\alpha T) v_j^\alpha. \tag{4}$$

In practice, three eigenvalues ($M=3$) can be determined along with their corresponding eigenvectors. These eigenvalues are identified with the masses of the $Q\bar{q}$ S-wave ground and radial excited states—up to a common additive constant due to the self-energy of the Q. This constant self-energy depends on the lattice formalism and hence only energy differences can be compared to possible experimental data such as the spectrum of B_s mesons that are basically $\bar{b}s$.

The techniques used to determine $C(2)$ are then extended to the corresponding matrix for the three-point correlation function $C_{ij}(3)$. As will be discussed more fully in Sec. V C, the desired radial correlations $x^{\alpha\beta}(r)$ are extracted by fitting $C_{ij}(3,r)$ with the form

$$\sum_{\alpha=1}^{M} \sum_{\beta=1}^{M} v_i^\alpha \exp[-m_\alpha t_1] x^{\alpha\beta}(r) \exp[-m_\beta(T-t_1)] v_j^\beta, \tag{5}$$

where the m_α and v_i^α have the values determined from $C(2)$.

Details of the derivation of the following formulas for $C(2)$ and $C(3)$ are given in the Appendix.

A. Two-point correlation functions $C(2)$

Given the above light-quark propagators, the two-point correlation functions $C(2)$ needed for extracting the energies of a heavy-light meson can be expressed in the four ways shown in Fig. 1. These are all the same up to statistical errors, but their combination improves the overall measurement. In Figs. 1(a) and (b), the heavy (static) quark propagator from site $(\mathbf{x}, t)$ to site $(\mathbf{x}', t+T)$ is simply
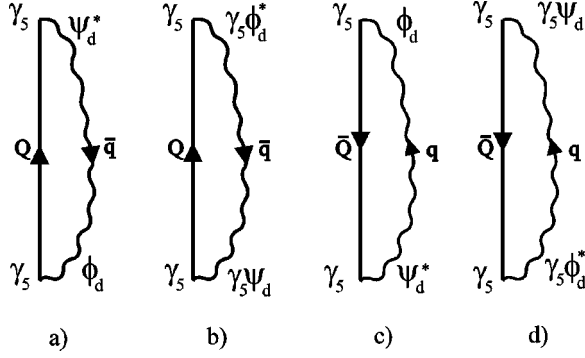
FIG. 1. The four contributions to the two-point correlation function $C(2)$.

$$G_Q(\mathbf{x},t;\mathbf{x}',t+T)=\frac{1}{2}(1+\gamma_4)U^Q(\mathbf{x},t,T)\delta_{\mathbf{x},\mathbf{x}'}, \qquad (6)$$

where $U^Q(\mathbf{x},t,T)=\prod_{i=0}^{T-1}U_4(\mathbf{x},t+i)$ is the gauge link product in the time direction. As shown in the Appendix this leads to the expression

$$C(2,T)=2\left\langle \operatorname{Re}\left[U^Q\left(\sum_{e=3,4} \psi_e^*(\mathbf{x},t+T)\phi_e(\mathbf{x},t) \right.\right.\right.$$
$$\left.\left.\left. + \sum_{d=1,2} \phi_d^*(\mathbf{x},t+T)\psi_d(\mathbf{x},t) \right) \right] \right\rangle, \qquad (7)$$

where d and e are Dirac spin indices.

B. Three-point correlation functions $C(3)$

The construction of the three-point correlation functions $C(3)$ follows that of $C(2)$ and they are depicted in Fig. 2. Since a probe is now inserted at a distance r from the heavy quark (Q), two light-quark propagators enter—one from Q to the probe and a second from the probe back to Q. The purpose of the probe is to measure the charge or matter distribution at a definite point $\mathbf{r}$. Therefore, only those light-quark propagators that involve the local basic field ϕ at $\mathbf{r}$ can be used, since the ψ field contains contributions from ϕ fields at next-to-nearest neighbor sites and so is *nonlocal*. Later, when fuzzing is introduced similar restrictions will enter. In this work two probes are studied: (i) $\Theta(\mathbf{r})=\gamma_4$ which measures the charge distribution (actually the light
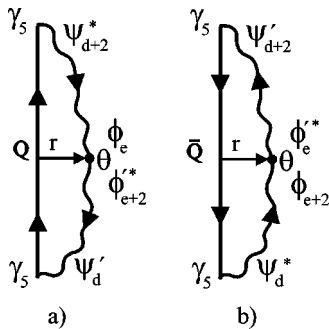
FIG. 2. The two contributions to the three-point correlation function $C(3)$.

quark charge normalized to 1) and (ii) $\Theta(\mathbf{r})=1$ which measures the matter distribution of the light quark.

As shown in the Appendix, the same techniques introduced to evaluate $C(2)$ can be extended to $C(3)$ giving the overall three-point correlation function as

$$C(3,-t_2,t_1,\mathbf{r})=C^Q(3)\mp C^{\bar{Q}}(3)$$
$$=2\langle X_R^q Y_R^Q - X_I^q Y_I^Q\rangle, \qquad (8)$$

where the X^q and Y^Q can be expressed in terms of $\phi\phi$ and $\psi U \psi$, respectively. In Eq. (8) the appropriate sign enters for $\Theta(\mathbf{r})=\gamma_4$, since the q and $\bar{q}$ have opposite charges.

IV. ANALYSIS

The correlations of interest are essentially obtained from the ratio $\langle C(3,T)\rangle/\langle C(2,T)\rangle$ by projecting out the ground state expectation value. However, the latter is only achieved in the limit $T\to\infty$. In practice, on a given lattice at the maximum possible values of T, the signal to noise ratio becomes large and effects from excited states are present. In order to reduce this contamination, a set of wave functions is constructed by fuzzing the original local wave function. These wave functions generate a better hadron operator where the $Q\bar{q}$ meson is created and destroyed. Then, together with the original local form, they serve as a variational basis for analyzing the data.

A. The effect of fuzzing

Fuzzing enters in two ways.

Firstly, the basic links containing the gauge field have two fuzzings. In the standard notation of, for example Ref. [8], Fuzz1 has 2 iterations and Fuzz 2 6 iterations. In both cases, the factor multiplying the basic link is $f_p=2.5$ i.e., [A fuzzed link] $=f_p\cdot$ [Straight link] + [Sum of 4 spatial U bends].

The pseudofermion field ϕ at a given lattice site $\mathbf{r}$ is considered to have three forms:

(1) The basic form that is simply a function of the single lattice site $\mathbf{r}$.

(2) The field at $\mathbf{r}$ is an average of the fields on the neighboring six lattice sites (i) i.e.

$$\phi_1(\mathbf{r})=\sum_i U(\text{Fuzz1},\mathbf{r},\mathbf{r}_i)\phi(\mathbf{r}_i).$$

(3) The field at $\mathbf{r}$ is an average of the fields on the six lattice sites (j) that are *two* lattice spacings from $\mathbf{r}$ i.e.

$$\phi_2(\mathbf{r})=\sum_j U(\text{Fuzz 2},\mathbf{r},\mathbf{r}_j)\phi(\mathbf{r}_j).$$

Therefore, only the basic field is local (L)—with $\phi_{N=1}$ and $\phi_{N=2}$ being increasingly non-local. This means that in the calculation of the above three-point correlation functions, only the basic ϕ field should be used at $\mathbf{r}$—the position of the probe insertion. There are now two reasons for this: (1) The field on the boundary at $t=0$ must be local. (2) The operator insertion must be local. This restriction does not

occur elsewhere, so that the ψ fields, which connect directly to the heavy quark, can be the fuzzed forms constructed from $Q_{ik}\phi_N$. This means that the two- and three-point correlation functions have the same size (3×3) as the overall correlation matrix, $LL, LF_1, LF_2, F_1F_1, F_1F_2$, and F_2F_2.

B. The variational method

There are many ways of analyzing the above correlations in order to extract the quantities of interest i.e. energies and wave functions. Here a variational method described in Ref. [9] is applied.

First, the two-point correlation data $C(2)$ are analyzed to give the energies (m_α) and eigenvectors ($\mathbf{v}$) for the $Q\bar{q}$ system. These are then used in analyzing the three-point correlation data $C(3)$ to give the charge and matter densities.

Consider the correlation function $C(2,T)$ as an $n\times n$ matrix—upto 3×3 in this case with the elements $LL, LF_1, \ldots, F_2F_2$. Each element $C_{ij}(2,T)$ is then fitted with the form

$$C_{ij}(2,T) \approx \tilde{C}_{ij}(2,T) = \sum_{\alpha=1}^{M} v_i^\alpha \exp(-m_\alpha T) v_j^\alpha, \quad (9)$$

where m_1 is the ground state energy of the heavy-light meson. The statistically independent matrix elements of $C(2)$ are then fitted by varying the $v_{i,j}^\alpha$ and m_α to minimize the difference between $C(2)$ and $\tilde{C}(2)$.

We illustrate the procedure for the 2×2 case, where the $C(2)$ can be expressed as the product of three 2×2 matrices:

$$C(2) = c^T \begin{pmatrix} \exp(-m_1 T) & 0 \\ 0 & \exp(-m_2 T) \end{pmatrix} c,$$

$$\text{where} \quad c = \begin{pmatrix} v_L^1 & v_{F1}^1 \\ v_L^2 & v_{F1}^2 \end{pmatrix} \quad (10)$$

and c^T is the transpose of c. In Ref. [9] the rows of c are called the $\mathbf{v}$ vectors v_i^α. Once the c matrix is known, any 2×2 correlation matrix C can be evaluated for the ground (excited) state wave function corresponding to the extracted eigenvalue m_1 (m_2) by reversing the above procedure to give

$$\bar{C} = (c^T)^{-1} C c^{-1} \quad \text{i.e.} \quad \bar{C}_{\alpha\beta} = u_i^\alpha C_{ij}(T) u_j^\beta, \quad (11)$$

where the u_i^α are components of the $\mathbf{u}$ vectors in Ref. [9]. These $\mathbf{u}$ vectors are the columns of the c^{-1} matrix and satisfy the condition

$$v_i^\alpha u_i^\beta = \delta_{\alpha\beta}. \quad (12)$$

For the 2×2 case

$$\mathbf{u}^1 = [v_{F1}^2, -v_L^2]/\det(c), \quad \mathbf{u}^2 = [-v_{F1}^1, v_L^1]/\det(c). \quad (13)$$

In the case where C is the above two-point correlation function $C(2)$ and $\tilde{C}$ in Eq. (9) is a perfect fit to C, then the operation in Eq. (11) would result in $\bar{C}$ being diagonal with the diagonal elements simply being $\exp(-m_\alpha T)$. Of course, in practice, the fit is never perfect and the off-diagonal elements of $\bar{C}$ are a measure of this goodness of fit. This will be demonstrated later. However, as pointed out in Ref. [9], for other correlation functions there is no reason for $\bar{C}$ to be diagonal.

V. RESULTS

The results are presented in two distinct parts. First, the two-point correlation function is analyzed to give the ground and excited state energies and eigenvectors i.e., m_1, m_2 in Eq. (10) and $\mathbf{u}^1, \mathbf{u}^2$ in Eq. (11). Secondly, these eigenvectors are used to extract the charge and matter radial distributions from the three-point correlation functions.

The actual pure gauge configurations (20 in number) and the pseudofermion fields ϕ (24 per gauge configuration) were taken from the tabulation generated for the work of Ref. [11]. These are for a $16^3\times 24$ lattice with $\beta=5.7$ with the Sheikholeslami-Wohlert improved clover action with $c_{SW}=1.57$—corresponding to a lattice spacing of $a \approx 0.17$ fm—and a hopping parameter $\kappa=0.14077$. The latter corresponds roughly to the strange quark mass. This can be seen from Ref. [13] where the same parameters in the light-light system ($q\bar{q}$) predict a vector meson to pseudoscalar meson mass ratio corresponding to strange quarks. More details can be found in Ref. [7].

In general, when we make fits to our lattice data with the MIGRAD option of MINUIT, we minimize χ^2 to achieve a reasonable value of χ^2/n_{dof}. The errors quoted on parameters are from the χ^2 increase when varying that parameter with all other parameters refitted. The systematic error on the fitted parameters comes mainly from the data set chosen (especially T_{min}) and we present results for different values of T_{min} to explore this.

In this study, we do not extrapolate the light quark mass to the physical case of u and d quarks, but retain it at around the strange quark mass. We also use an infinite heavy quark mass. Thus our study pertains to $\bar{Q}s$ mesons where Q is a very heavy (so static) quark. For this case the remaining systematic errors come from the lack of sea-quark effects and the finite lattice spacing used. Although we use a tadpole-improved fermion formalism which should reduce lattice artifacts, it will be necessary to repeat our calculations at smaller lattice spacing in order to extrapolate to the continuum limit and so quantify this source of error. We are using the quenched approximation in this study, and evaluations with sea quark effects included will be needed to explore the effects of this approximation on our results.

A. Analysis of the two-point correlation function $C(2)$

Essentially the energies (E), in lattice units, are extracted from the $C(2,T)$ in Eq. (7) using
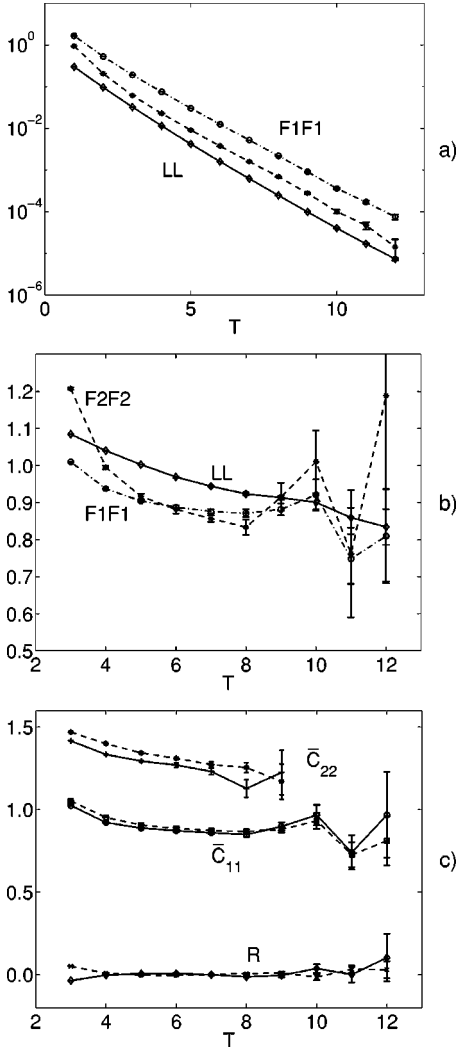
FIG. 3. (a) The basic LL, $F1F1$, and $F2F2$ elements of $C(2)$. (b) The values of $E(T)$ for LL, $F1F1$, and $F2F2$ separately. (c) The combinations of $L, F1, F2$ for cases 3 (solid) and 4 (dashed) to give $E[\bar{C}_{\alpha\alpha}]$. Also shown is the ratio $R = \langle \bar{C}_{12}(2,T) \rangle / \langle \bar{C}_{11}(2,T) \rangle$ defined in Eq. (15).

$$E[C(2,T)] = -\ln\left[\frac{\langle C(2,T) \rangle}{\langle C(2,T-1) \rangle}\right] \quad \text{as} \quad T \to \infty. \quad (14)$$

In Fig. 3(a) the basic $C(2,T)$ are plotted for the three diagonal matrix elements where the fields are (i) purely local (L), (ii) all Fuzz1, (iii) all Fuzz 2, in the notation of Sec. IV A. They are all seen to be well determined with the errors being significant only for Fuzz 2 with $T > 10$. In Fig. 3(b) the results $E[C_{ii}(2,T)]$ from Eq. (14) are plotted for the three sets of diagonal matrix elements with $i = L, F1, F2$. There it is seen that only $E[C_{F1F1}(2,T)]$ shows a clean plateau that extends from $T = 5$ to 9 with a value about 0.88(1).

To combine these results by a variational calculation using Eq. (9) two numbers are fixed:

(i) M—the number of energies being included. Here, this is taken to be the same as the number of paths for each energy and results in the correlation matrices being square.

(ii) T_{min}—the minimum value of T used in the fit.

Here we consider four possibilities to check the dependence of the final results on this fitting procedure:

Case 1. In Eq. (9), the $\tilde{C}_{ij}(T)$ are defined in terms of 3 paths (i.e. $i, j = 1,2,3$) and 3 exponentials (i.e. $M = 3$) with $T_{min} = 3$. This includes the local and both Fuzz1 and Fuzz 2 paths.

Case 2. The same as case 1 but with 2 paths and 2 exponentials. This includes only the local and Fuzz1 paths.

Cases 3,4 are the same as cases 1,2 but with $T_{min} = 4$.

Minimizing the difference between $C(2,T)$ and $\tilde{C}(2,T)$ in Eq. (9) gives the parameters in Table I. These are surprisingly good fits, when it is realized that the errors on $C(2,T)$ are, in most cases, much less than 1%. However, only case 3 gives $\chi^2/n_{dof}(2) < 1$ and so this is the one that will be used in most of this study.

In Fig. 3(c) the results for $E[\bar{C}_{\alpha\alpha}]$ from Eq. (14) are plotted for the two sets of diagonal matrix elements $\bar{C}_{11}(2,T)$ and $\bar{C}_{22}(2,T)$ for cases 3 and 4. As expected, $E[\bar{C}_{11}(2,T)] \approx 0.86(2)$ and $E[\bar{C}_{22}(2,T)] \approx 1.24(5)$—energies that are consistent with the values of m_1 and m_2 in Table I. As a check on the off-diagonal matrix element $\bar{C}_{12}(2,T)$, we evaluate

$$R[\bar{C}_{12}(2,T)] = \frac{\langle \bar{C}_{12}(2,T) \rangle}{\langle \bar{C}_{11}(2,T) \rangle}. \quad (15)$$

This is seen to be at the 1% level. The conclusion to be drawn from Fig. 3(c) is that $\bar{C}$ is, indeed, approximately diagonal with $\bar{C}_{\alpha\beta}(2,T) \approx \exp(-m_\alpha T)\delta_{\alpha\beta}$. These results will serve as a comparison when analyzing $C(3,T,r)$ later.

From Table I, the main result of this subsection—and the one used in most of this study–is case 3 for the 3×3 fit using $C(2)$ data with $T \geq 4$. Case 4 is for the 2×2 fit with $T \geq 4$. This is also used in some later analyses, but is considered to be inferior to case 3. Cases 1 and 2 are given to show that the inclusion of the $T = 3$ data significantly worsens the fit.

B. Analysis of the three-point correlation function for sum rules

The charge and matter radial distributions $F(r, \Theta)$ of the light quark in the $Q\bar{q}$ system are extracted using

$$F[C(\Theta, T, r)] = \frac{\langle C(3, \Theta, T, r) \rangle}{\langle C(2, T) \rangle}, \quad (16)$$

where $\Theta = \gamma_4$ or 1. However, before showing these radial distributions, it is of interest to first study the corresponding sum rules

$$F^{sum}[C(\Theta, T)] = \frac{\sum_{\mathbf{r}} \langle C(3, \Theta, T, \mathbf{r}) \rangle}{\langle C(2, T) \rangle}$$
$$= \frac{\langle C^{sum}(3, \Theta, T) \rangle}{\langle C(2, T) \rangle}, \quad (17)$$

TABLE I. Values of the parameters am_α and v_i^α, where $a \approx 0.17$ fm is the lattice spacing. Cases 1–4 fit the two point correlations $[C(2)]$.

am_α $v_i^\alpha u_i^\alpha$	Case 1 3×3 $T_{min}=3$	Case 2 2×2 $T_{min}=3$	Case 3 3×3 $T_{min}=4$	Case 4 2×2 $T_{min}=4$
am_1	0.8849(10)	0.9005(14)	0.8721(19)	0.8833(27)
am_2	1.2953(63)	1.355(10)	1.263(13)	1.307(20)
am_3	1.99(10)		1.94(30)	
v_L^1	0.5164(30)	0.5574(41)	0.4847(56)	0.5149(82)
v_{F1}^1	1.5892(48)	1.6761(52)	1.519(10)	1.589(13)
v_{F2}^1	0.8651(22)		0.8402(38)	
v_L^2	0.8123(61)	$-0.8226(74)$	0.816(16)	$-0.834(19)$
v_{F1}^2	0.435(22)	$-0.065(29)$	0.644(49)	$-0.373(57)$
v_{F2}^2	$-0.393(18)$		$-0.251(33)$	
v_L^3	$-0.258(63)$		$-0.28(22)$	
v_{F1}^3	1.93(32)		2.2(1.4)	
v_{F2}^3	$-1.40(24)$		$-1.13(81)$	
$n_{data}(2)$	60	30	54	27
$n_{param}(2)$	12	6	12	6
$n_{dof}(2)$	48	24	42	21
$\chi^2/n_{dof}(2)$	3.1	7.5	0.65	1.15
u_L^1	0.0421	-0.0480	-0.0608	-0.3294
u_{F1}^1	0.3546	0.6126	0.3258	0.7361
u_{F2}^1	0.4793		0.6364	
u_L^2	1.1135	-1.2482	1.1575	-1.4024
u_{F1}^2	-0.1432	0.4151	-0.1025	0.4545
u_{F2}^2	-0.4016		-0.4825	

where $\Sigma_\mathbf{r}$ represents the sum over all spatial lattice sites at time $t=0$—the time when the probe acts. The summation can be easily carried out exactly on the lattice. For the charge distribution this sum rule should, *in the continuum limit*, simply yield the charge of the light quark, which we have chosen to normalize to unity. For the matter distribution the situation is less clear—see Refs. [2,3].

In Fig. 4(a) we show $F^{sum}[C_{ii}(\gamma_4,T)]$ for the three cases $i=L,F1,F2$. There it is seen that, at large T, the sum rule for $i=L$ becomes 1.05(5) and so is consistent with unity. However, the results for $i=F1,F2$ appear to be somewhat greater than unity for $T>5$ converging to 1.25(5) and 1.4(1). When these results are combined using the **u** vectors in Table I, then—as seen in Fig. 4(b)—the ground state sums $F^{sum}[\bar{C}_{11}(\gamma_4,T)]$ for both cases 3 and 4 are dominated by the $F^{sum}[C_{F1F1}(\gamma_4,T)]$. Consequently, they are again distinctly greater than unity with both cases 3 and 4 tending to about 1.30(5). This seems unavoidable since, as seen from Table I, the **u** vector components u_{F1}^1 and u_{F2}^1 are an order of magnitude larger than u_L^1. In Fig. 4(b) the sum rule for the first excited state $F^{sum}[\bar{C}_{22}(\gamma_4,T)]$ is also shown. This appears to be approaching unity at about $T\approx7$–8. However, the signal is swamped by the error bars at larger T.

The correlations $C_{ij}^{sum}(3)$ are not so well diagonalized as the $C_{ij}(2)$ were forced to be earlier. A measure of this is plotted in Fig. 4(b) as

$$R^{sum}[\bar{C}_{12}(\Theta,T)] = \frac{\langle\bar{C}_{12}^{sum}(3,\Theta,T)\rangle}{\langle\bar{C}_{11}^{sum}(3,\Theta,T)\rangle}. \qquad (18)$$

This is seen to be at the 10% level—an order of magnitude larger than the corresponding $R[\bar{C}_{12}(2,T)]$ in Eq. (15). Therefore, it is seen that the γ_4 sum rule calculated in the above way has two undesirable features:

(1) The ground state sum rule $F^{sum}[\bar{C}_{11}(\gamma_4,T)]$ is not consistent with unity for large T, being more like 1.30(5). Only in the continuum limit should the sum be unity. To some extent this must be expected, since in the present non-continuum situation the lattice vector current is not conserved. In principle this can be corrected in various ways. Unfortunately, at the present value of $\beta=5.7$, perturbative expressions would exhibit poor convergence and so be unreliable. Nonperturbative corrections are discussed in the recent review in Ref. [10]. There an improved vector operator is introduced and calculations performed in the quenched approximation at $\beta=6.2$ and 6.0. However, they find that, whereas the $\beta=6.2$ results are satisfactory, those at $\beta=6.0$ are not—suggesting that $O(a^2)$ discretization errors are not small at the larger lattice spacing. The situation would be even worse at the value of $\beta=5.7$ used here. Even so, it is illustrative to see the results at the higher β's, since they may indicate what could possibly be expected at lower β's. In
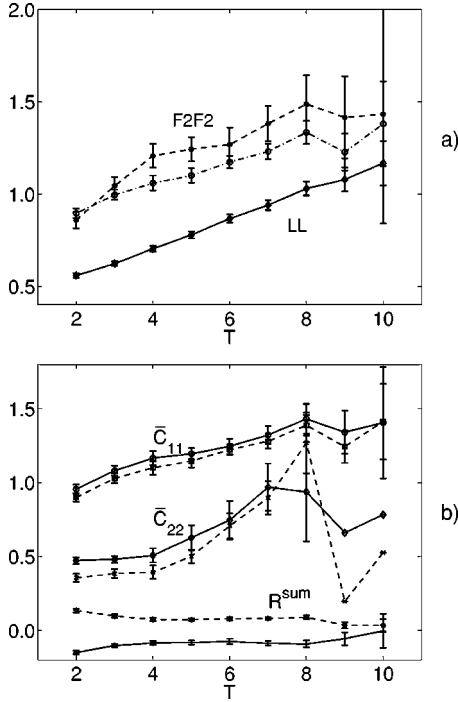
FIG. 4. The γ_4 sum rule: (a) contributions LL, $F1F1$ and $F2F2$ separately; (b) the combinations of $L,F1,F2$ for cases 3 (solid) and 4 (dashed) to give $F^{sum}[\bar{C}_{\alpha\alpha}(\gamma_4,T)]$ defined in Eq. (17) and R^{sum} in Eq. (18).

Ref. [10], when the expectation value of the renormalized vector current is expressed as

$$\langle J^R \rangle = F^V \langle \gamma_4(x) \rangle, \tag{19}$$

where $\langle \gamma_4(x) \rangle$ is the quantity evaluated in Eq. (17), the authors find that $F^V \approx 0.8$. Similar reductions are found in Ref. [1] for the axial vector operator. Of course, the above argument could be reversed to say that the present charge sum rule measurement of 1.30(5) gives a nonperturbative estimate of F^V as 0.77(3). Later, when individual radial contributions are extracted as in Eq. (16), this continuum effect could be incorporated approximately by the renormalization

$$F[\bar{C}_{\alpha\alpha}(\gamma_4,T,r)] \rightarrow \frac{F[\bar{C}_{\alpha\alpha}(\gamma_4,T,r)]}{F^{sum}[\bar{C}_{\alpha\alpha}(\gamma_4,T)]}. \tag{20}$$

(2) The off-diagonal terms, as illustrated by $R^{sum}[\bar{C}_{12}(\gamma_4,T)]$ in Eq. (18), are not zero. However, zero is only necessary in the continuum limit, when neglecting pair creation. Also, as will be shown in the next subsection, where radial distributions are extracted, we find that about *half* of the contributions to the sum rule lie inside $r \approx 2$. At such small values of r, lattice artifacts may well play a role to give a non-zero value for R^{sum}.

So far the basic wave functions u_i^α have been determined, from Eq. (9), via the v_i^α i.e. by considering only the two-point correlations $C(2)$. In an attempt to overcome the two above problems with $F^{sum}[\bar{C}(\gamma_4,T)]$, the analysis of the data is now carried out by fitting not only $C(2)$ but also some features of $C(3)$.

In analogy to Eq. (9) the sum rule data are fitted with the expression

$$C_{ij}^{sum}(3,\gamma_4,T) \approx \tilde{C}_{ij}^{sum}(3,\gamma_4,T)$$

$$= \sum_{\alpha=1}^{M} \sum_{\beta=1}^{M} v_i^\alpha \exp[-m_\alpha t_1] x^{\alpha\beta}$$

$$\times \exp[-m_\beta(T-t_1)]v_j^\beta, \tag{21}$$

where the v_i^α are from Table I—the earlier result of minimizing the $C_{ij}(2)$—but the $x^{\alpha\beta}$ are treated as free parameters. However, a restriction must be made on the values of T used in Eq. (21). From Table I it is seen that T_{min} must be at least 4 to ensure that $\chi^2(2)/n_{dof}(2)$ is comparable to unity. Therefore, in $C^{sum}(3)$ each of the two propagators should be at least 4 Euclidean time steps, i.e., in Eq. (21) we should have $t_1 \geq 4$ and $(T-t_1) \geq 4$. This means that only the $C(3,T)$ data with $T_{min}(3) \geq 8$ should be included in any fitting procedure. However, in the following a series of $T_{min}(3)$ values, ranging from 4 to 9, are used to see how the final results depend on $T_{min}(3)$. Therefore, in case 3, i.e. 3×3 with $T_{min}(3) = 4$ (8), this involves fitting 42 (18) pieces of data with 6 parameters and in case 4, i.e. 2×2 with $T_{min}(3) = 4$ (8), this involves fitting 21 (9) pieces of data with 3 parameters. In Table II, the results for χ^2/n_{dof} are shown separately for the fits to $C(2)$ and $C^{sum}(3)$. There for case 3 it is seen that—as with $\chi^2(2)/n_{dof}(2)$—the $\chi^2(3)/n_{dof}(3)$ are also ≈ 1 provided $T_{min}(3) \geq 6$. This result can be compared directly with Fig. 4(b), since it is simply an alternative analysis under similar constraints. It is seen that the values of $x^{11} = 1.35(5)$ and $x^{22} \approx 1$ are indeed consistent with the asymptotic values of F^{sum} in Fig. 4(b). On the other hand, x^{12} cannot be compared directly with $R^{sum}[\bar{C}_{12}(\gamma_4,T)]$ in Eq. (18). All that can be said there is that both analyses result in nonzero and negative values for x^{12}.

In an attempt to overcome this last point, in cases $3'$ and $4'$, all three off diagonal terms $x^{\alpha\beta}$ are fixed at zero. For a given $T_{min}(3)$, this decreases x^{11} but at the expense of increasing $\chi^2(3)/n_{dof}(3)$. The outcome is that for $\chi^2(3)/n_{dof}(3) < 1$ with $x^{12} = 0$ and $T_{min}(3) = 8$ we get $x^{11} = 1.29(3)$—a number consistent with 1.30(5) from Fig. 4(b). However, x^{22} changes violently, even though the plot corresponding to Fig. 4 (b) is very similar—with, in particular, $F^{sum}[\bar{C}_{22}(\gamma_4,T)]$ again approaching unity and not zero as would be expected from the value for x^{22} in Table II. To check this last unexpected result, the analysis program was run using the *model* results $\tilde{C}_{ij}^{sum}(3,\gamma_4,T)$ instead of the lattice data $C_{ij}^{sum}(3,\gamma_4,T)$. The plot corresponding to Fig. 4(b) now has for the excited state $F^{sum}[\bar{C}_{22}(\gamma_4,T)] \approx 0.005$ for all values of T — consistent with Table II. This difference for x^{22} demonstrates the need to try to improve $\chi^2(3)/n_{dof}(3)$ at smaller values of $T_{min}(3)$. It appears that the results for the excited states are very dependent on the **v** vectors, since they involve delicate cancellations. Of course, the main concern is the consistency between x^{11} and $F^{sum}[\bar{C}_{11}(\gamma_4,T)]$ and this emerges intact.

TABLE II. Values of $x^{\alpha\beta}$ for cases 3 and 3'. In case 3 the 12 parameters describing $C(2)$ are fixed and only the 6 $x^{\alpha\beta}$ are varied to fit $C(3)$. In case 3' only the 3 $x^{\alpha\alpha}$ are varied. The superscript * implies that the number is fixed at this value. The entries denoted by a dash cannot be accurately determined.

	Case 3			Case 3'		
$\chi^2(2)/n_{dof}(2)$	0.65*			0.65*		
$T_{min}(3)$	4	6	8	4	6	8
$\chi^2(3)/n_{dof}(3)$	1.20	0.72	0.26	4.2	2.4	0.68
x^{11}	1.26(2)	1.33(2)	1.41(5)	1.12(1)	1.19(1)	1.29(3)
x^{12}	$-0.32(3)$	$-0.44(7)$	$-0.5(2)$	0*	0*	0*
x^{13}	0.03(9)	0.0(3)	0(1)	0*	0*	0*
x^{22}	0.65(7)	0.9(2)	0.9(9)	0.00(4)	$-0.3(1)$	$-1.2(4)$
x^{23}	0.2(2)	0(1)	0(8)	0*	0*	0*
x^{33}	0.2(9)	4(8)	–	$-0.3(8)$	1(7)	–
	Case 4			Case 4'		
$\chi^2(2)/n_{dof}(2)$	1.15*			1.15*		
$T_{min}(3)$	4	6	8	4	6	8
$\chi^2(3)/n_{dof}(3)$	1.23	0.78	0.21	3.4	2.0	0.58
x^{11}	1.24(2)	1.29(3)	1.36(7)	1.10(1)	1.17(2)	1.26(3)
x^{12}	$-0.36(5)$	$-0.45(11)$	$-0.5(3)$	0*	0*	0*
x^{22}	0.65(13)	0.8(4)	1(2)	$-0.19(5)$	$-0.6(2)$	$-1.6(6)$

In the above, the data for $C_{ij}(2,T)$ and $C_{ij}^{sum}(3,\gamma_4,T)$ were fitted separately. Therefore, now a combined fit is made using Eqs. (9) and (21) i.e. for case 3 (3') with $T_{min}=4$, $T_{min}(3)=8$, this involves fitting $54+18$ pieces of data for $C(2)+C(3)$ with $12+6$ (3) parameters. However, this has a completely negligible effect e.g. in case 3, $T_{min}=4$, $T_{min}(3)=8$ the values of $\chi^2(2)/n_{dof}(2),\chi^2(3)/n_{dof}(3)$ and $\chi^2(2+3)/n_{dof}(2+3)$ change from 0.647, 0.718, 0.673 to 0.652, 0.699, 0.669 and x^{11} from 1.3274(249) to 1.3274(255). The conclusion is that for the sum rules there is no benefit in fine tuning the results by simultaneously fitting $C(2)$ and $C(3)$.

The main result from this subsection is the value of the ground state sum rule $x^{11}=1.29$ (3) in Table II for case 3' with $T_{min}(3)=8$. This particular value is preferred, since it involves the best fit (case 3) from Table I and also constrains the off-diagonal elements $x^{\alpha\beta}$ to be zero—as expected in the continuum limit.

C. Analysis of the three-point correlation function for the charge radial distributions

In Figs. 5(a) and 5(b) are shown, for $r/a=0,\ldots,5$, the ratios

$$F[\bar{C}_{11}(\gamma_4,T,r)]=\frac{\langle\bar{C}_{11}(3,\Theta=\gamma_4,T,r)\rangle}{\langle\bar{C}_{11}(2,T)\rangle}, \qquad (22)$$

based on Eq. (16) using the **v** vectors of case 3. These all exhibit, to a certain extent, a plateau as T becomes large. However, for $r/a>5$ the error bars become very large be-

yond $T=8$. No attempt will be made at this stage to extract the asymptotic values giving the radial distributions.

The second procedure for analyzing the radial distribution three-point correlation functions $C(3,\theta,T,r)$ is similar to the
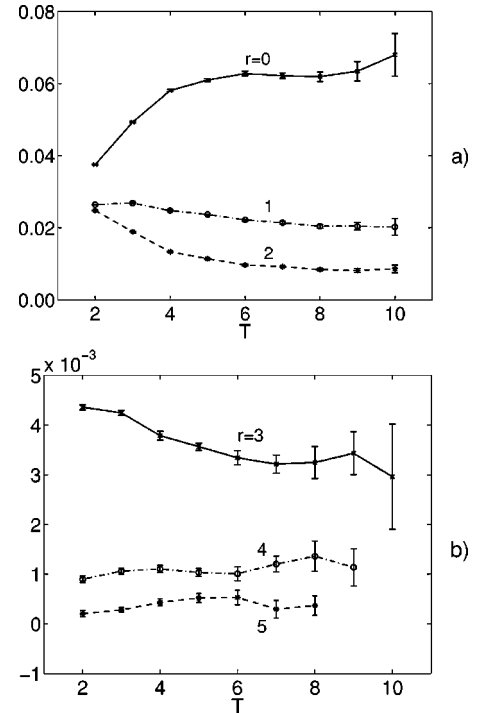
FIG. 5. The ratio $\langle C(3,r)\rangle/\langle C(2)\rangle$ for case 3. (a) $r=0,1,2$ and (b) $r=4,5,6$ in lattice units $a\approx0.17$ fm.

TABLE III. The ground and first excited state charge densities x^{11}, x^{22} for different values of $T_{min}(3)$. In case 3 only the six $x^{\alpha\beta}(r)$ are varied—the **v** vectors being those determined earlier from fitting $C(2)$ and shown in Table I. In case $3'$ only the three $x^{\alpha\alpha}(r)$ are varied. The numbers in square brackets are the $\chi^2(3)/n_{dof}(3)$. The entries denoted by a dash have unreasonably large $\chi^2(3)/n_{dof}(3)$. The interquark distance r is in lattice units of $a \approx 0.17$ fm.

x^{11}, Case 3	$r=0$	$r=1$	$r=2$	$r=3$	$r=4$	$r=5$
$T_{min}(3)=6$	0.0627(2)	0.0214(1)	0.00906(8)	0.00328(6)	0.00112(6)	0.00031(6)
	[0.37]	[2.54]	[2.37]	[0.20]	[0.40]	[0.82]
$T_{min}(3)=7$	0.0629(3)	0.0209(2)	0.00882(10)	0.00326(9)	0.00120(9)	0.00021(8)
	[0.27]	[1.67]	[1.49]	[0.25]	[0.34]	[0.59]
$T_{min}(3)=8$	0.0633(5)	0.0204(2)	0.0084(2)	0.0033(1)	0.0012(1)	0.00017(11)
	[0.16]	[1.38]	[0.36]	[0.33]	[0.49]	[0.68]
$T_{min}(3)=9$	0.0631(7)	0.0200(4)	0.0081(2)	0.0033(2)	0.0010(2)	$-0.0002(2)$
	[0.24]	[1.48]	[0.05]	[0.48]	[0.53]	[0.39]
x^{11}, Case $3'$	$r=0$	$r=1$	$r=2$	$r=3$	$r=4$	$r=5$
$T_{min}(3)=7$	–	–	0.00856(5)	0.00287(4)	0.00100(5)	0.00018(5)
	–	–	[2.09]	[1.87]	[0.94]	[0.58]
$T_{min}(3)=8$	–	–	0.0084(1)	0.0029(1)	0.0010(1)	0.00012(7)
	–	–	[0.38]	[1.08]	[0.67]	[0.81]
$T_{min}(3)=9$	–	–	0.0082(1)	0.0029(1)	0.0009(1)	0.0000(1)
	–	–	[0.07]	[0.80]	[0.37]	[0.33]
x^{22}, Case 3	$r=0$	$r=1$	$r=2$	$r=3$	$r=4$	$r=5$
$T_{min}(3)=6$	0.192(3)	0.011(1)	0.0019(7)	0.0009(5)	0.0004(6)	0.0003(6)
$T_{min}(3)=8$	0.19(1)	0.010(4)	0.001(3)	0.001(2)	0.000(3)	0.001(2)
x^{22}, Case $3'$	$r=0$	$r=1$	$r=2$	$r=3$	$r=4$	$r=5$
$T_{min}(3)=7$	–	–	$-0.001(1)$	$-0.0033(4)$	$-0.0020(6)$	0.000(1)

one followed above but using the expression

$$C_{ij}(3,\gamma_4,T,r) \approx \tilde{C}_{ij}(3,\gamma_4,T,r)$$

$$= \sum_{\alpha=1}^{M} \sum_{\beta=1}^{M} v_i^\alpha \exp[-m_\alpha t_1] x^{\alpha\beta}(r)$$

$$\times \exp[-m_\beta(T-t_1)] v_j^\beta, \quad (23)$$

analogous to Eq. (21) for the sum rule but with all the r dependence being put into the $x^{\alpha\beta}(r)$. Two types of fit are made:

The **v** vectors, obtained by minimizing the $C(2)$, are used in Eq. (23) and for each value r the $x^{\alpha\beta}(r)$ are varied to ensure a good fit to $C_{ij}(3,\gamma_4,T,r)$ by the model form $\tilde{C}_{ij}(3,\gamma_4,T,r)$.

A simultaneous fit of $C_{ij}(2,T)$ and $C_{ij}(3,\gamma_4,T,r)$ is made using $\tilde{C}_{ij}(2,T)$ and $\tilde{C}_{ij}(3,\gamma_4,T,r)$ of Eqs. (9) and (23).

To achieve a $\chi^2(2+3)/n_{dof}(2+3) \approx 1$ is now more difficult than with the earlier $C(2),C^{sum}(3)$ fit, since the $C_{ij}(3,\gamma_4,T,r)$ have error bars that are smaller than the corresponding sum rule correlations. For example, the most important correlations $i=j=F1$ have the values $C(2,T=4) =0.0752(3)$ and $C(3,T=8,r/a=2)=0.0000528(9)$ compared with $C^{sum}(3,T=8)=0.029(1)$ i.e. the errors on $C(2)$ are $\approx 0.5\%$, those on $C^{sum}(3)$ are $\approx 5\%$, but those on $C(3,r)$ are only 2%. This is seen in Table III, where in

particular for $r/a=1$ the values of $\chi^2(3)/n_{dof}(3)$ are all greater than unity. In this table it is also seen that the radial distribution of the ground state charge density, $x^{11}(r)$, is well determined and is consistent with the plateaus in Figs. 5(a) and (b). When the $x^{11}(r)$ are plotted on a semilogarithmic scale as in Fig. 6, the distribution for $r/a \lesssim 4$ is approximately a straight line suggesting that $w_c(r)=A_c\exp(-r/r_c)$, where $w_c^2(r)=x^{11}(r)$. The function $w_c(r)$ is then interpreted as a radial wave function. However, the other diagonal matrix element, $x^{22}(r)$, is much less well determined—as is seen in the lower half of Table III. In fact, for some values of r, it appears to be slightly negative. But the actual values are very small and could well be consistent with zero. Only for case 3 at $r/a=0$ is there a definite signal with $x^{22}(0) \approx 0.19$. This suggests that $x^{22}(r)$ is very sharply peaked compared with $x^{11}(r)$. However, it must be remembered that in case 3 the off-diagonal terms $x^{\alpha\beta}(r)$ are not forced to be zero and so the interpretation of $x^{22}(r)$ is not clear. In case $3'$ where the off-diagonal terms $x^{\alpha\beta}(r)$ are forced to be zero, no signal can be extracted at $r=0$. There is certainly no sign of a node that would be expected of an excited S wave.

Figure 6 also suggests that for $r/a \gtrsim 4$ the function $w(r)$ drops off faster than the above simple exponential. Such an effect is expected at sufficiently large r when the linear rising confining potential becomes important. Then as $r \to \infty$ the wave function should have an $\exp[-(r/r_1)^{3/2}]$ asymptotic
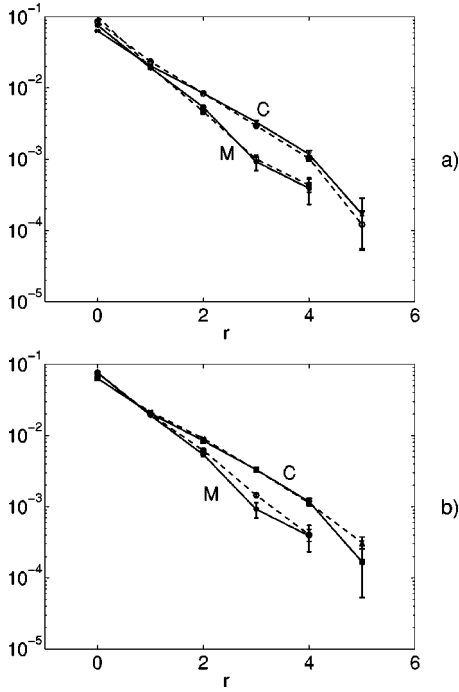
FIG. 6. The radial distribution of the ground state charge (C) and matter (M) densities $x^{11}(r)$. (a) Cases 3 (solid) and 3′ (dashed) with $T_{min}(3)=8$; (b) case 3 for $T_{min}(3)=8$ (solid) and 6 (dashed). The interquark distance (r) is in lattice units $a\approx0.17$ fm.

form. Unfortunately, for $r/a>5$ the errors on the data become too large, so that the above observation rests completely on the $r/a=5$ data, which themselves are rather poor. Even so, there the errors are still sufficiently small to support this. It is planned to extend the present calculation to off-axis

points. The $r/a=5$ results can then be checked by performing simulations at $x/a=3,y/a=4$. The resulting data should be more accurate since each (x,y) pair arises in 24 different ways—not just 6 as for the on-axis points with $r\neq0$.

The actual parameters defining $w_c(r)$ can be extracted in a variety of ways depending on $T_{min}(3)$ and the range of r values used in the fit. But as seen in Table IV they appear to be quite stable for cases 3 and 3′ separately. For case 3 $A_c \approx0.23(1)$ and $r_c/a\approx2.1(1)$ and for case 3′ $A_c\approx0.26(1)$ and $r_c/a\approx1.9(1)$. Given these numbers, estimates of the sum rule are $I_c=\int_0^\infty d\mathbf{r}w_c^2(r)=\pi A_c^2 r_c^3$. These are shown in the last column of Table IV and are all 1.6(1) for case 3 and 1.5(1) for case 3′. The corresponding numbers for the sum rule obtained directly from the lattice and shown in Table II are 1.35(5) and 1.25(5), respectively. This difference between the two methods is not surprising, since the integrand in $I_c=\int_0^\infty d\mathbf{r}w_c^2(r)$ is maximum at $r/a\approx2$ and half of the sum I_c lies inside this value of r. Therefore, lattice artifacts, present at small values of r, may play a role. These are expected to affect I_c more than the direct results of Table II—a point that can be checked by estimating x^{11} away from axes e.g. not only at $(\pm1,0,0),(0,\pm1,0),(0,0,\pm1)$ but also at $(\pm1,\pm1,0)$ etc.

In addition to fitting the $x^{11}\approx w_c^2(r)$ with simply the two parameter function $w_c(r)=A_c\exp(-r/r_c)$, attempts were made with the three parameter function $w_c(r)=A_c\exp[-(r/r_c)^p]$. As seen in Table IV, this results in values of p that are somewhat greater than unity—as expected from Fig. 6 where the $r/a=5$ point appears to drop below the earlier simple exponential. This also has the effect of decreasing the value of $I_c=\int_0^\infty d\mathbf{r}w_c^2(r)$ from the simple exponential value of $\pi A_c^2 r_c^3$. However, since about 90% of I_c comes from r values less than 5, this in practice can have only a minor effect.

TABLE IV. The parametrization of the wave function as $w_c(r)=A_c\exp[-(r/r_c)^p]$ for various values of $T_{min}(3)$ and ranges of r. Also given is $I=\pi A_c^2 r_c^3$. Here only fits with $\chi^2/dof\approx1$ are reported. The cases with $p=1^*$ have p fixed. Both A_c and r_c are expressed in terms of lattice units $a\approx0.17$ fm.

Case 3	r range	A_c	r_c	p	I
$T_{min}(3)=7$	2–4	0.254(7)	2.01(5)	1^*	1.52(14)
	1–4	0.199(5)	2.87(14)	1.23(5)	1.52
$T_{min}(3)=8$	1–4	0.225(3)	2.20(4)	1^*	1.71(10)
	2–4	0.238(10)	2.10(8)	1^*	1.65(23)
	1–4	0.208(11)	2.59(25)	1.13(9)	1.56
$T_{min}(3)=9$	1–4	0.224(4)	2.18(6)	1^*	1.64(15)
	1–4	0.202(15)	2.66(37)	1.16(14)	1.47
	1–5	0.196(12)	2.81(31)	1.22(12)	1.41
Case 3′					
$T_{min}(3)=7$	2–4	0.275(4)	1.84(2)	1^*	1.47(6)
	1–4	0.249(5)	2.12(8)	1.08(3)	1.43
$T_{min}(3)=8$	1–4	0.257(2)	1.94(2)	1^*	1.50(5)
	2–4	0.261(6)	1.91(4)	1^*	1.49(12)
	1–4	0.250(9)	2.04(13)	1.03(4)	1.47
$T_{min}(3)=9$	1–4	0.251(2)	1.96(3)	1^*	1.49(7)
	2–4	0.260(10)	1.90(7)	1^*	1.46(20)
	1–4	0.237(12)	2.19(21)	1.08(7)	1.41

TABLE V. Values of $x^{\alpha\beta}$ in cases 3 and 3′ for the *matter* distribution. Notation as in Table II.

	Case 3			Case 3′		
$\chi^2(2)/n_{dof}(2)$		0.65*			0.65*	
$T_{min}(3)$	4	6	8	4	6	8
$\chi^2(3)/n_{dof}(3)$	0.40	0.45	0.35	0.72	0.43	0.29
x^{11}	0.56(3)	0.49(6)	0.38(15)	0.48(2)	0.45(3)	0.35(7)
x^{12}	−0.22(7)	−0.1(2)	−0.1(5)	0*	0*	0*
x^{13}	−0.2(2)	0.0(8)	−1(5)	0*	0*	0*
x^{22}	0.4(2)	0.4(5)	1(2)	−0.11(9)	0.0(3)	0(1)
x^{23}	0.3(4)	0(3)	–	0*	0*	0*
x^{33}	2(2)	–	–	2(2)	–	–

Assuming the simple exponential form, an estimate of the mean-square charge radius is $\langle r^2 \rangle = 3r_c^2$ in lattice units of $a \approx 0.17$ fm. For cases 3 and 3′ this gives 0.38(3) and 0.32(1) fm^2, respectively.

The main results from this subsection are the ground state radial correlations $x^{11}(r)$ and their parametrization for $T_{min}(3) = 8$ in Tables III and IV. If the off-diagonal elements $x^{\alpha\beta}(r)$ are constrained to be zero, then only correlations for $r = 2,3,4,5$ can be extracted with a reasonable χ^2/n_{dof}. However, these correlations are consistent with those of case 3, where the off-diagonal elements are not constrained. This suggests that the values at $r = 0$ and 1 for case 3 are, in fact, similar to those for case 3′.

D. Analysis of the three-point correlation function for the matter radial distributions

The previous two subsections have dealt with the charge radial distribution, where the operator Θ in Eq. (22) is γ_4 for probing the $\bar{q}$ charge. In this subsection $\Theta = 1$, which probes the $\bar{q}$ matter.

In Table V the values of the $x^{\alpha\beta}$ in cases 3 and 3′ are given. Here it is seen that x^{11} the matter sum rule for the ground state is more erratic than its charge counterpart in Table II—a point clearly seen in the corresponding plot in Fig. 7. A reasonable estimate for x^{11} is 0.4(1). This value is consistent with the corresponding estimates in Refs. [3] and [7] for $12^3 \times 24$ lattices. These were made by employing data
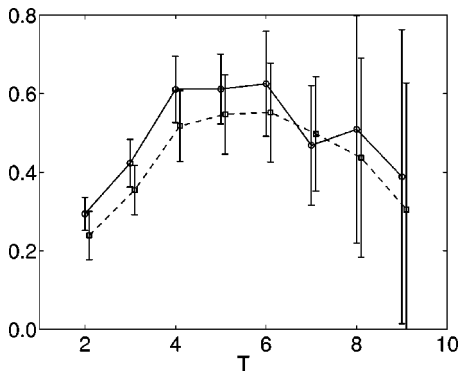
FIG. 7. Matter sum rule with cases 3 (solid) and 4 (dashed) $L, F1, F2$ combinations.

from different hopping parameters (κ) and using the identity

$$x^{11} = \frac{d(am_1)}{d\kappa^{-1}}, \quad (24)$$

where am_1 is the ground state energy and κ the hopping parameter—see Ref. [2]. When the m_1's correspond to the cases where the light meson is of about one and two strange quark masses, Refs. [3] and [7] give 0.34(8) and 0.31(6), respectively—consistent with the present value of 0.4(1).

These larger values are also consistent with the following simple estimate—again using the above identity in Eq. (24). If the $Q\bar{q}$-meson mass (am_1) is taken to be simply the sum of the quark masses $am_Q + am_q$ and $\kappa^{-1} = 8 + 2am_q$, then

$$x^{11} = \frac{d(am_Q + am_q)}{d(8 + 2am_q)} = 0.5. \quad (25)$$

Another reason for expecting $x^{11} < 1$ also follows from a potential approach using the Dirac equation. If the $\bar{q}$ is treated as a particle in a potential generated by the Q, then its wave function will be of the form (f, g), where f (g) are the large (small) components of the Dirac wave function. The charge of the $\bar{q}$ will then be simply $I_C = \int d\mathbf{r}[f^2(r) + g^2(r)]$, which by the normalization will be unity. However, when the charge operator (γ_4) is replaced by the matter operator (unity), the corresponding integral is now $I_M = \int d\mathbf{r}[f^2(r) - g^2(r)]$. In the nonrelativistic limit $I_C = I_M$. But as relativistic effects enter i.e. g^2 increases from zero, then I_M becomes less than I_C i.e. less than unity. An indication of this is seen in the lattice results in Table 10.3 in Ref. [3], where x^{11} decreases from 0.21(8) to 0.11(5) as the $\bar{q}$ mass decreases from about two to one strange quark masses. This also shows—as expected—that the interquark potential is more than one-gluon exchange ($-\alpha/r$), since the latter results in $g/f = (1 - \gamma)/\alpha$, where $\gamma = \sqrt{1 - \alpha^2}$—a ratio that is independent of the light quark mass—see, for example, [12]. For $\alpha = 0.3$ this gives $g/f = 0.15$—a number that is much smaller than the ≈ 0.75 suggested by the charge and matter sum rules measured above on the lattice.

In Table VI the matter densities are given in analogy with the charge densities of Table III. Comparison of these two

TABLE VI. The matter densities with notation as in Table III.

x^{11}, Case 3	$r=0$	$r=1$	$r=2$	$r=3$	$r=4$	$r=5$
$T_{min}(3)=6$	0.0758(3)	0.0199(1)	0.0062(1)	0.00145(8)	0.00040(8)	0.00004(7)
	[0.20]	[1.07]	[0.83]	[0.83]	[0.23]	[0.60]
$T_{min}(3)=8$	0.0758(7)	0.0192(3)	0.0054(3)	0.0009(3)	0.0004(2)	0.0005(2)
	[0.25]	[0.04]	[0.19]	[0.94]	[0.19]	[0.06]
x^{11}, Case 3$'$	$r=0$	$r=1$	$r=2$	$r=3$	$r=4$	$r=5$
$T_{min}(3)=6$	–	–	–	0.00113(4)	0.00034 (4)	0.00003(5)
	–	–	–	[1.82]	[0.24]	[0.57]
$T_{min}(3)=8$	–	0.0196(2)	0.0046(2)	0.0010(1)	0.00043(9)	0.0003(1)
	–	[1.24]	[0.80]	[0.77]	[0.16]	[0.16]

tables shows that the ground state matter distribution $x(\text{matter})=x_m^{11}$ decays faster than the corresponding ground state charge distribution $x(\text{charge})=x_c^{11}$. At $r=0$ the two are comparable but, by $r/a=4$, $x(\text{matter})$ is only 25% of $x(\text{charge})$. This is also seen in Fig. 6. Now the $r/a=5$ data are even more uncertain than the earlier charge data. They are, therefore, not quoted.

Table VII shows the parameters A_m and r_m when $w_m(r)$ is parametrized as $w_m(r)=A_m\exp(-r/r_m)$. There it is seen that A_c, for the charge distribution, and A_m are comparable, but that $r_m/a\approx1.55(5)$ compared with the charge range of $r_c/a\approx2.0$. This difference between r_c and r_m means that the interpretation that $w_c(r)$ and $w_m(r)$ are both $\bar{q}$ wave functions is not so direct, since in the most naive models one would expect $w_c(r)=w_m(r)$.

The main points from this subsection are that: (1) From Table V, the matter sum rule x^{11} for the ground state is 0.4(1); (2) from Tables VI and VII the most realistic results are for case 3$'$ with $T_{min}(3)=8$. These show that the matter distribution wave function $[w_m(r)]$ has a significantly shorter range [0.24(2) fm] than the corresponding charge [0.32(2) fm].

VI. CONCLUSION

In this paper a first study has been made of the radial structure of a heavy-light meson—the quark equivalent of the hydrogen atom. This can be considered as a partial extension of Ref. [7] in which only the energies of heavy-light

mesons were measured on a lattice. Here the emphasis is on the charge and matter radial distributions. So far these distributions have been extracted only for the ground state, with the extension to other partial waves—as in Ref. [7]—only now beginning to be studied. A further extension would be a study of the form of the underlying color fields that lead to these radial correlations. This would be analogous to the studies in Refs. [6] for the $(Q\bar{Q})$ and $(Q^2\bar{Q}^2)$ systems.

The main result is in Fig. 6, where it is seen that both the charge and matter radial distributions fall off more or less exponentially as $A_i^2\exp[-2r/r_i]$. The amplitudes A_i are about the same with $A_c\approx0.26(1)$ and $A_m\approx0.29(1)$, whereas the charge range $r_c/a\approx1.9(1)$ is considerably longer than the matter range $r_m/a\approx1.4(1)$. This difference is reflected in the spatial sum rule, which is about 1.30(5) for the charge and 0.4(1) for the matter. The fact that the charge sum rule is not unity, as would be expected from vector current conservation, can be attributed to the finite spacing of the lattice. As shown in Refs. [1] and [10] this can easily lead to 10–20 % reductions.

It should be added that there are other definitions of $Q\bar{q}$ wave functions. Here the relative wave function $[w(r)]$ is assumed to be real with $w^2(r)$ giving the charge density — the quantity actually measured from $\langle C(3,T)\rangle/\langle C(2,T)\rangle$. Another form can be extracted directly from a two-point correlation function in which the operators at the sink and source are of spatial sizes r_1 and r_2, respectively. The ground state correlation can then be fitted with

TABLE VII. The parametrization of the matter distribution wave function as $w_m(r)=A_m\exp[-r/r_m]$. Notation as in Table IV.

Case 3	r range	A_m	r_m	I_m
$T_{min}(3)=6$	2–4	0.33(2)	1.40(5)	0.92(14)
$T_{min}(3)=8$	0–4	0.275(1)	1.46(2)	0.75(3)
	1–4	0.271(8)	1.49(5)	0.77(9)
	2–4	0.37(8)	1.24(16)	0.81(46)
Case 3$'$	r range	A_m	r_m	I_m
$T_{min}(3)=6$	1–4	0.293(2)	1.39(1)	0.72(2)
$T_{min}(3)=8$	1–4	0.287(5)	1.39(3)	0.69(5)

$w_{BS}(r_1)w_{BS}(r_2)\exp(-m_1T)$ to give $w_{BS}(r)$, which can be identified with the Bethe-Salpeter wavefunction—see Ref. [7].

The above charge and matter radial densities are related by a simple Fourier transform to the momentum space vector and scalar form factors $[F_{v,s}(q^2)]$ of the B meson. Unfortunately, the present densities are not accurate enough over a sufficiently large range of r to perform this transform. However, a simple model of these form factors is that they are dominated by the pole due to the lightest meson of mass m i.e. they have a form $\propto(q^2+m^2)^{-1}$. On the lattice with our parameters and quark mass, it is found that the lightest vector and scalar meson masses are $am_v=0.815(5)$ and $am_s=1.39(5)$, respectively—see Refs. [9,13]. The Fourier transform of these pole terms is then a Yukawa form $\propto\exp(-mr)/r$, which—in principle—can now be compared directly with the charge and matter radial densities measured here. However, it is only the asymptotic form that should be used in this comparison since that will be controlled by the lightest particle mass. But from Fig. 6 it is seen that the present data extend only up to $r/a=5$ (4) for the charge (matter) density, corresponding to $mr=0.4$ (0.6), respectively, which is not large. Furthermore, the charge density is already well described by a simple exponential up to $r/a=4$ and so a comparably good fit over this range by a Yukawa form is ruled out. As a compromise, since the charge density data are somewhat better than those for the matter density, the charge densities at $r/a=3$ and 4 are used to extract estimates of m_v and the matter densities at $r/a=2$ and 3 for an estimate of m_s. Case 3 leads to $am_v=0.7(1)$ and $am_s=1.4(4)$—the corresponding numbers for case $3'$ being 0.8(1) and 1.1(1). Even though these estimates are qualitatively consistent with the lattice results of Refs. [13,9], it should be added that they are dependent on the range of r values used.

This paper should be considered only as the first step in measuring densities. Many extensions and refinements are possible:

In the $Q\bar{q}$ system, the measurement of the $P_{1/2},P_{3/2},D_{3/2},D_{5/2}$, etc., densities corresponding to the energies extracted in Ref. [7]. For a given orbital angular momentum, do these correlations show the degeneracy predicted in Ref. [14]?

Off-axis radial correlations. These would check not only rotational invariance but also the radial correlation for $r/a=5$, which could then be measured at, for example, $x/a=3,y/a=4$ etc. This point is of particular interest, since in Fig. 6 there is a hint that the correlation is lower than that obtained from a simple extrapolation. Such a lowering is expected, when the linear confining potential begins to play a role.

The measurement of correlations in the baryonic and $(Q^2\bar{q}^2)$ system. Are these similar to those in the $(Q\bar{q})$ case—as is the case when comparing correlations in few-nucleon systems?

The replacement of quenched by unquenched gauge configurations. This is not expected to have a significant effect on the charge sum rule and correlations. However, as discussed in Refs. [2,3], for the matter probe disconnected contributions arise that are dependent on quenched versus unquenched configurations. The difference between the two could highlight the effect of the quark condensate.

The use of larger β values and lattices to check the continuum limit of the present results.

The use of several light quark masses to enable an attempt at extrapolating to the realistic nonstrange light quark masses.

Other one body operators. In this work only the charge (γ_4) and matter (1) probes have been studied. However, others are of interest—see, for example, Ref. [1] where the pseudovector operator $(\gamma_\mu\gamma_5)$ is needed for the $B^*B\pi$ coupling.

APPENDIX: THE CORRELATION FUNCTIONS $C(2)$ AND $C(3)$

This appendix gives details of the derivations of Eqs. (7) and (8) for the two- and three-point correlation functions $C(2)$ and $C(3)$.

1. Two-point correlation functions $C(2)$

Given the light-quark propagators in Eqs. (2) and (3), the two-point correlation functions $C(2)$ can be expressed in the four ways shown in Fig. 1. These are the same up to statistical errors, but their combination improves the overall measurement.

Case a: The $Q\bar{q}$ meson with the propagator in Eq. (2).

Case b: The $Q\bar{q}$ meson with the propagator in Eq. (3).

Case c: The $\bar{Q}q$ meson with the propagator in Eq. (2).

Case d: The $\bar{Q}q$ meson with the propagator in Eq. (3).

In cases a and b, the heavy (static) quark propagator from site $(\mathbf{x},t)$ to site $(\mathbf{x}',t+T)$ is simply

$$G_Q(\mathbf{x},t;\mathbf{x}',t+T)=\frac{1}{2}(1+\gamma_4)U^Q(\mathbf{x},t,T)\delta_{\mathbf{x},\mathbf{x}'},\quad(\text{A1})$$

where $U^Q(\mathbf{x},t,T)=\Pi_{i=0}^{T-1}U_4(\mathbf{x},t+i)$ is the gauge link product in the time direction. On the other hand, for cases c and d, the heavy(static)-antiquark propagator from site $(\mathbf{x},t)$ to site $(\mathbf{x}',t+T)$ is simply

$$G_{\bar{Q}}(\mathbf{x},t;\mathbf{x}',t+T)=\frac{1}{2}(1-\gamma_4)U^{Q\dagger}(\mathbf{x},t,T)\delta_{\mathbf{x},\mathbf{x}'}.\quad(\text{A2})$$

The general form of a two-point correlation is constructed from a heavy-quark propagating from site $(\mathbf{x}_1,t)$ to site $(\mathbf{x}_1',t+T)$ and a light-quark propagating from site $(\mathbf{x}_2,t+T)$ to site $(\mathbf{x}_2',t)$ i.e.

$$C(2,T) = \text{Tr}\langle \Gamma^\dagger G_Q(\mathbf{x},t;\mathbf{x}',t+T)\Gamma G_q(\mathbf{x},t+T;\mathbf{x}',t)\rangle, \tag{A3}$$

where Γ is the spin structure of the heavy-quark light-quark vertices at t and $t+T$. In this case, since the B meson is a pseudoscalar, we have $\Gamma = \gamma_5$. These definitions lead to the four two-point correlation functions

$$C(2,T,a) = \sum_{d=3,4} \langle U^Q(\mathbf{x},t,T)\psi_d^*(\mathbf{x},t+T)\phi_d(\mathbf{x},t)\rangle \tag{A4}$$

$$C(2,T,b) = \sum_{d=1,2} \langle U^Q(\mathbf{x},t,T)\phi_d^*(\mathbf{x},t+T)\psi_d(\mathbf{x},t)\rangle \tag{A5}$$

$$C(2,T,c) = \sum_{d=1,2} \langle U^{*Q}(\mathbf{x},t,T)\psi_d^*(\mathbf{x},t)\phi_d(\mathbf{x},t+T)\rangle \tag{A6}$$

$$C(2,T,d) = \sum_{d=3,4} \langle U^{*Q}(\mathbf{x},t,T)\phi_d^*(\mathbf{x},t)\psi_d(\mathbf{x},t+T)\rangle, \tag{A7}$$

where d is the Dirac spin index. We see that $C(2,T,c)^* = C(2,T,b)$ and $C(2,T,d)^* = C(2,T,a)$, so that the sum leads to

$$C(2,T) = 2\left\langle \text{Re}\left[U^Q\left(\sum_{e=3,4} \psi_e^*(\mathbf{x},t+T)\phi_e(\mathbf{x},t) \right.\right.\right.$$
$$\left.\left.\left. + \sum_{d=1,2} \phi_d^*(\mathbf{x},t+T)\psi_d(\mathbf{x},t) \right)\right]\right\rangle. \tag{A8}$$

2. Three-point correlation functions $C(3)$

The construction of the three-point correlation functions $C(3)$ follows that of $C(2)$ and they are depicted in Fig. 2.

Consider that the probe is at $t=0$ and that Q propagates from $(\mathbf{x},-t_2)$ to $(\mathbf{x},t_1)$. Analogous to Eq. (A3), the general form of $C(3)$—when involving a Q—is then

$$C^Q(3,-t_2,t_1,\mathbf{r}) = \text{Tr}\langle \Gamma^\dagger G_Q(\mathbf{x},-t_2;\mathbf{x},t_1)\Gamma G_q(\mathbf{x},t_1;\mathbf{x} \right.$$
$$\left. +\mathbf{r},0)\Theta(\mathbf{r})G_q'(\mathbf{x}+\mathbf{r},0;\mathbf{x},-t_2)\rangle. \tag{A9}$$

This combination of the G_q and G_q' defined in Eqs. (2), (3) ensures that only the local field ϕ occurs at the probe position $\mathbf{r}$. When $\Theta(\mathbf{r}) = \gamma_4$, this expression reduces to

$$C^Q(3,-t_2,t_1,\mathbf{r}) = \left\langle \left[\sum_{d=1,2} U^Q \psi_{d+2}^*(\mathbf{x},t_1)\psi_d'(\mathbf{x},-t_2) \right]\right.$$
$$\times \left[\sum_{e=1,2} \phi_e(\mathbf{x}+\mathbf{r},0)\phi_{e+2}'^*(\mathbf{x}+\mathbf{r},0) \right.$$
$$\left.\left. - \phi_{e+2}(\mathbf{x}+\mathbf{r},0)\phi_e'^*(\mathbf{x}+\mathbf{r},0) \right]\right\rangle. \tag{A10}$$

Care must be exercised here, since $\phi_e(\mathbf{x}+\mathbf{r},0)$ arises from G_q, whereas $\phi_e'^*(\mathbf{x}+\mathbf{r},0)$ is from G_q', and so the two cannot be combined. The last equation can now be written as

$$C^Q(3,-t_2,t_1,\mathbf{r}) = \langle [X_R^q+iX_I^q][Y_R^Q+iY_I^Q]\rangle, \tag{A11}$$

where, suppressing color indices

$$X_R^q = \sum_{e=1,2} [\phi_e(R)\phi_{e+2}'(R) + \phi_e(I)\phi_{e+2}'(I)$$
$$\mp \phi_{e+2}(R)\phi_e'(R) \mp \phi_{e+2}(I)\phi_e'(I)]$$

$$X_I^q = \sum_{e=1,2} [\phi_e(I)\phi_{e+2}'(R) - \phi_e(R)\phi_{e+2}'(I)$$
$$\pm \phi_{e+2}(R)\phi_e'(I) \mp \phi_{e+2}(I)\phi_e'(R)], \tag{A12}$$

where the upper signs are for $\Theta(\mathbf{r}) = \gamma_4$ and the lower ones for $\Theta(\mathbf{r}) = 1$. Suppressing color and spin indices,

$$Y_R^Q = \psi'(R)U(R)\psi(R) + \psi'(I)U(R)\psi(I) - \psi'(I)U(I)\psi(R)$$
$$+ \psi'(R)U(I)\psi(I)$$

$$Y_I^Q = -\psi'(R)U(R)\psi(I) + \psi'(I)U(R)\psi(R)$$
$$+ \psi'(I)U(I)\psi(I) + \psi'(R)U(I)\psi(R). \tag{A13}$$

When involving a $\bar{Q}$, the corresponding three-point correlation function is

$$C_3^{\bar{Q}}(-t_2,t_1,\mathbf{r}) = \text{Tr}\langle \Gamma G_{\bar{Q}}(\mathbf{x},t_1;\mathbf{x},-t_2)\Gamma^\dagger G_q(\mathbf{x},-t_2;\mathbf{x}$$
$$+\mathbf{r},0)\Theta(\mathbf{r})G_q'(\mathbf{x}+\mathbf{r},0,\mathbf{x};t_1)\rangle, \tag{A14}$$

which can be written in the notation of Eq. (A11) as

$$C^{\bar{Q}}(3,-t_2,t_1,\mathbf{r}) = \langle [-X_R^q+iX_I^q][Y_R^Q-iY_I^Q]\rangle. \tag{A15}$$

The overall three-point correlation function is then

$$C(3,-t_2,t_1,\mathbf{r}) = C^Q(3)\mp C^{\bar{Q}}(3) = 2\langle X_R^q Y_R^Q - X_I^q Y_I^Q\rangle, \tag{A16}$$

where the negative sign enters for $\Theta(\mathbf{r}) = \gamma_4$, since the q and $\bar{q}$ have opposite charges.

[1] G.M. de Divitiis, L. Del Debbio, M. Di Pierro, J.M. Flynn, C. Michael, and J. Peisa, J. High Energy Phys. **10**, 010 (1998).

[2] UKQCD Collaboration, M. Foster and C. Michael, Phys. Rev. D **59**, 074503 (1999).

[3] M. Foster, Ph.D. thesis, University of Liverpool, 1998.

[4] T.A. Lähde, C.J. Nyfält, and D.O. Riska, Nucl. Phys. **A674**, 141 (2000). M. Di Pierro and E. Eichten, Phys. Rev. D **64**, 114004 (2001).

[5] W. Glöckle and H. Kamada, Phys. Rev. Lett. **71**, 971 (1993); M. Baldo *et al.*, NuPECC report, 2000.

[6] P. Pennanen, A.M. Green, and C. Michael, Phys. Rev. D **59**, 014504 (1999); **56**, 3903 (1997); G.S. Bali, K. Schilling, and C. Schlichter, *ibid.* **51**, 5165 (1995).

[7] C. Michael and J. Peisa, Phys. Rev. D **58**, 034506 (1998).

[8] A.M. Green, C. Michael, and J.E. Paton, Nucl. Phys. **A554**, 701 (1993).

[9] UKQCD Collaboration, C. McNeile and C. Michael, Phys. Rev. D **63**, 114503 (2001).

[10] K.C. Bowler, L. Del Debbio, J.M. Flynn, G.N. Lacagnina, V.I. Lesk, C.M. Maynard, and D.G. Richards, hep-lat/0007020.

[11] UKQCD Collaboration, C. Michael and P. Pennanen, Phys. Rev. D **60**, 054012 (1999); UKQCD Collaboration, C. Michael, P. Pennanen, and A.M. Green, in Lattice '99, Proceedings of the 17th International Symposium on Lattice Field Theory, Pisa, Italy [Nucl. Phys. B (Proc. Suppl.) **83-84**, 200 (2000)], hep-lat/9908032; P. Pennanen and C. Michael, hep-lat/0001015.

[12] J.D. Bjorken and S.D. Drell, *Relativistic Quantum Mechanics* (McGraw-Hill, New York, 1964).

[13] UKQCD Collaboration, H. Shanahan *et al.*, Phys. Rev. D **55**, 1548 (1997).

[14] P.R. Page, T. Goldman, and J.N. Ginocchio, Phys. Rev. Lett. **86**, 204 (2001).